Desalination and Water Treatment
www.deswater.com
doi: 10.5004/dwt.2021.26985

220 (2021) 211–220
April

Novel thin film nanocomposite forward osmosis membrane embedded with amine functionalized UiO-66 metal organic frameworks as an effective way to remove heavy metal Cr^{3+} ions

Tala Eghbalazar, Alireza Shakeri*, Alireza Abbasi

School of Chemistry, College of Science, University of Tehran, P.O. Box: 14155-6619, Tehran, Iran, Tel. +98 (21) 61113812; Fax: +98 (21) 66972047; email: alireza.shakeri@ut.ac.ir

Received 21 July 2020; Accepted 27 December 2020

ABSTRACT

This research work reports a simple and novel method to fabricate thin film nanocomposite forward osmosis membranes (TFN-FO). The newly designed TFN membrane was fabricated by incorporation of $UiO_{66}^{NH_2}$ nanoparticles within a polyamide thin film by using the interfacial polymerization (IP) of *m*-phenylenediamine/aminated (MPD/$UiO_{66}^{NH_2}$) aqueous and trimesoyl chloride (TMC) organic solution. Then, the morphology characteristics, water permeability, and removal behavior of Cr^{3+} ions were thoroughly evaluated. Compared with the unmodified thin film composite (TFC) membrane, the $UiO_{66}^{NH_2}$ modified TFN-U_{800} membrane (800 ppm nanofiller concentration) presented higher hydrophilicity and better overall FO performance. Additionally, the TFN-U_{800} membrane exhibited greater metal removal for heavy metal Cr^{3+} ions in AL-FS mode (feed solution in contact with active layer) than the control TFC membrane, arising from its improved polyamide (PA) layer characteristic. We expect that this novel technique can be applied to fabricate TFN-FO membranes with good heavy metal separation performance.

Keywords: Heavy metal; Thin film nanocomposite; Forward osmosis; Active layer

1. Introduction

With the rapid growth of diverse industry centers, such as electronics, mining, machinery manufacturing, metallurgy, and electroplating, considerable amounts of wastewater containing heavy metals have been discarded into water resources in different ways [1,2]. Unlike other noxious materials, heavy metal ions are highly stable and cannot be degraded [3,4]. For this reason, they are stored in living organisms, which cause major hazards both physiologically and ecologically [5]. So, it is essential to eliminate heavy metals from wastewater by using proper treatment prior to discharging the environment. A variety of methods, such as adsorption, ion exchange, chemical precipitation, reduction/oxidation, and membrane separation, for example, nanofiltration (NF) and reverse osmosis (RO), have been developed to remove heavy metal ions-containing wastewater [6–9]. Compared to other methods, the membrane process has some advantages, such as no phase changing, environmental friendly, and high separation efficiency. Meanwhile, although pressure-driven membrane processes are more advantageous than the traditional separation methods, limitations such as high energy consumption and fouling problem are still the most severe drawbacks which unfavorably affect heavy metal ions separation performance [9,10]. Recently, the forward osmosis (FO) process, as a hot research topic, has received lots of attention not only in seawater desalination but also in several water treatment techniques such as removal of trace organic compounds, separation of oily wastewater, and removal of heavy metal

* Corresponding author.

1944-3994/1944-3986 © 2021 Desalination Publications. All rights reserved.

ions [9–13]. In the FO separation process, solvent molecules spontaneously diffuse through a semipermeable asymmetric FO membrane from the feed solution side (FS, high solvent chemical potential) to the draw solution side (DS, low solvent chemical potential) while impeding the exchange of the solute [14]. Nowadays, state-of-the-art thin film composite (TFC) FO membranes consisting of a porous polymeric supporting layer and an ultrathin polyamide (PA) cross-linked layer are generally employed for FO process [14–16]. Although the compacted PA barrier layer provides high selectivity for the TFC membrane, a highly cross-linked network greatly restricts the permeation of water molecules [10]. Accordingly, in order to optimize the efficiency separation, the PA thin film should have an adjustable crosslinking density to obtain an excellent solute rejection and certain free volume for accelerating water molecules permeation [17]. As a result, there is a requirement for further careful design of FO-based membrane structure to maximize the FO separation performance. Currently, the so-called thin film nanocomposite (TFN) membrane fabricated by introducing nanofillers in the PA thin film during interfacial polymerization (IP) has been extensively employed to improve the separation performance of membranes [18–20]. A class of promising porous materials, termed as metal organic frameworks, (MOFs) has been widely employed for designing novel TFN membranes in diverse fields of membrane separation processes [21]. Compared with conventional packed-structure nanomodifiers, such as ZnO, TiO_2, and SiO_2, porous MOFs endow further passways for penetration of water molecules, which alleviates the mass transfer resistance and leads to an improvement in water permeability [22,23]. Among MOF nanomaterials, Zr-based framework ($UiO_{66}^{NH_2}$) seems to be appropriate for the fabrication of TFN membranes. The preparation of TFN membranes with $UiO_{66}^{NH_2}$, has several merits including (1) tuning wide pores, (2) good water stability and relatively high thermal stability, and (3) improving the compatibility and adhesion of $UiO_{66}^{NH_2}$ with the PA active layer due to the reaction of amine groups with acid chloride [24]. In this work, with respect to the excellent properties of $UiO_{66}^{NH_2}$, a defect-free PA thin film incorporated with $UiO_{66}^{NH_2}$ was synthesized for the efficiently removal of heavy metal Cr^{3+} ions. The effect of $UiO_{66}^{NH_2}$ on TFN surface hydrophilicity, chemical composition, and morphology of top layer as well as FO separation performance were also evaluated systematically. This work may anticipate a simple method to develop FO applications by designing the novel TFN-FO membrane.

2. Experimental section

2.1. Materials

The $UiO_{66}^{NH_2}$ metal-organic framework was fabricated by zirconium chloride ($ZrCl_4$, Sigma-Aldrich, USA) as metal ion source, 2-aminoterephthalic acid (NH_2–BDC, Sigma-Aldrich, USA) as organic ligand, *N*,*N*-dimethyl formaldehyde (DMF, Merck, USA) as solvent for synthesis and acetic acid (Merck, Germany) as the additives. Polyethersulfone (PES, BASF Co., Germany, M_w = 58,000 (as polymeric substrate, *N*-methyl-2-pyrrolidone (Merck, NMP, Germany) as solvent, polyethylene glycol with molecular weight of 400 (Merck, PEG-400, Germany) as a pore-forming agent and deionized (DI) water as non-solvent in the coagulation bath were employed for the fabrication of flat sheet substrates. In order to deposit PA active layer on the PES substrate, *m*-phenylenediamine (MPD, Sigma-Aldrich, USA), and trimesoyl chloride (TMC, Sigma-Aldrich, USA) were used as water-soluble and *n*-hexane (Merck, Germany) soluble monomer, respectively. For evaluation of FO performance, sodium chloride (NaCl, Iran Mineral Salts Company) were dissolved in DI water and used as a draw solution (Iran).

2.2. Synthesis of $UiO_{66}^{NH_2}$ nanoparticles

The $UiO_{66}^{NH_2}$ crystalline nanoparticles were prepared via the solvothermal method according to the previously reported procedure [25,26]. In brief, 0.52 g of $ZrCl_4$ and 0.17 g of NH_2BDC were dissolved in a mixed solution of DMF (10 mL) and acetic acid (0.1 mL) by sonication. After that, the obtained mixture solution was added into a 100 mL autoclave and kept in an oven at 120°C for 24 h. The $UiO_{66}^{NH_2}$ precipitate was isolated by centrifuging, followed by thorough rinsing with fresh DMF and methanol three times. Finally, the product was dried at 80°C in air and further activated at 150°C in a vacuum oven.

2.3. Preparation of FO support layer

The support layer membranes were fabricated by phase inversion method by using the similar procedure reported in our previous work [27]. For the preparation of PES membrane, dried PES (15 wt.%) and PEG-400 (20 wt.%) were dissolved in NMP (65 wt.%), and then, stirred at room temperature until a transparent dope solution was attained. After that, the casting solution was degassed over 24 h. Thereafter, the dope solution was cast over a pre-cleaned plate by using a blade with 100 μm in gap width, and then instantly by immersion into a DI water coagulation bath at room temperature to form the porous PES sublayer. Once the precipitated PES was peeled off from the glass plate, it was washed and stored in another DI water bath for at least 12 h prior to preparation of the TFN-FO membranes.

2.4. Synthesis of PA thin film

The skin PA active layer of the TFC membrane (control) was deposited on the PES supporting layer through the IP method in boundary of the aqueous and organic solutions. The PES support layer was washed with DI-water, and the top surface of the PES membrane was placed in contact with MPD solution (2 wt.%) for 2 min to ensure that the solution phase penetrates into the porous supporting layer. Residual drops of the solution were slowly removed from the top surface of the saturated substrate by using an air knife. Afterwards, the MPD-impregnated sublayer was gently immersed into TMC/*n*-hexane (0.1 wt.%) to form the PA rejection layer. After the accomplishment of the reaction between MPD and TMC for 1.5 min, the membrane was taken out of the organic phase, and then, crosslinking of PA was augmented in the oven at 60°C for 1 min. In the entire of the IP process, the membrane support layers were fixed between two frames so that the IP reaction could be

performed only at their top surfaces. Fabrication of $UiO_{66}^{NH_2}$-embedded TFN-FO membranes was similar to the unmodified TFC membrane, expect that the $UiO_{66}^{NH_2}$ nanoparticles was introduced into an aqueous phase beforehand. A predetermined amount of $UiO_{66}^{NH_2}$ (100–1,000 ppm) was dispersed in DI-water by sonicating for 1 h at 20°C, and MPD monomer was then dissolved in the $UiO_{66}^{NH_2}$ suspension. These $UiO_{66}^{NH_2}$ modified membranes were denoted as TFN-U_{100}, TFN-U_{200}, TFN-U_{400}, TFN-U_{800}, and TFN-U_{1000}, in which the number refers to the $UiO_{66}^{NH_2}$ concentration. The procedure used for the fabrication of $UiO_{66}^{NH_2}$-incorporated TFN membrane is schematically illustrated in Fig. 1.

2.5. FO performance tests

A bench-scale cross-flow separation cell with an effective surface area of 4.9 cm^2 was used to determine the reverse salt flux (J_s, gMH) and water flux (J_w, LMH) of the as-fabricated membranes (TFC and TFN) in FO (PA active layer faced with feed solution) configuration. For this assessment, both the DS (1 L of NaCl aqueous solution 1 mol/L) and FS (1 L of DI-water) were pumped at a cross-flow velocity of 100 mL/min on both side of the membrane [28]. Each fabricated membrane sample was tested at 25°C for at least three times to achieve a reliable average reverse salt flux and water flux data. J_w and J_s were determined by Eqs. (1) and (2), based on the effective membrane area (A_m, 4.9 cm^2) and the change in the feed solution volume (ΔV, L).

$$J_w = \frac{\Delta V t}{A \Delta t} \tag{1}$$

$$J_s = \frac{\Delta\left(C_t V_t\right)}{A \Delta t} \tag{2}$$

where V_t and C_t represent the feed volume (L) and the solute concentration (g/L) after a certain test time (Δt, h), respectively. An EC meter (Adwa, AD332) was used to analyze solute concentrations in the feed solution during the FO experiments.

2.6. Heavy metal ions removal test

The heavy metal ion removal performance of the as-prepared TFN-U800 membrane was examined under FO mode [6,29]. Cr^{3+}(aq) solutions (1 L) with different concentrations (500; 1,000; 1,500; and 2,000 ppm of $Cr(NO_3)_3$ were employed as the feed solution, and the 1.0 M aqueous solution of NaCl was used as the draw solution. The Cr^{3+} rejection (R_{Cr}) was determined by using Eq. (3):

$$R_{Cr} = \left(1 - \frac{C_d V_d}{C_f V_t}\right) \times 100\% \tag{3}$$

where V_d (L) and C_d (g/L) are the final volume of the draw solution and the concentration of Cr^{3+} in the draw solution, respectively. The original concentration of Cr^{3+} (g/L) in the feed side is C_f, while V_t (L) is the increased volume of the draw side. An inductively coupled plasma optical emission spectrometer (ICP-OES, OPTIMA2100DV) was used to calculate C_d after the FO process.

2.7. Characterization of $UiO_{66}^{NH_2}$ nanofiller

The chemical structure of $UiO_{66}^{NH_2}$ was studied by using Fourier transform infrared (FT-IR) spectroscopy (Bruker, Equinox 55) over the wavenumber ranging from 600 to 4,000 cm^{-1}. For characterization of the morphology and size

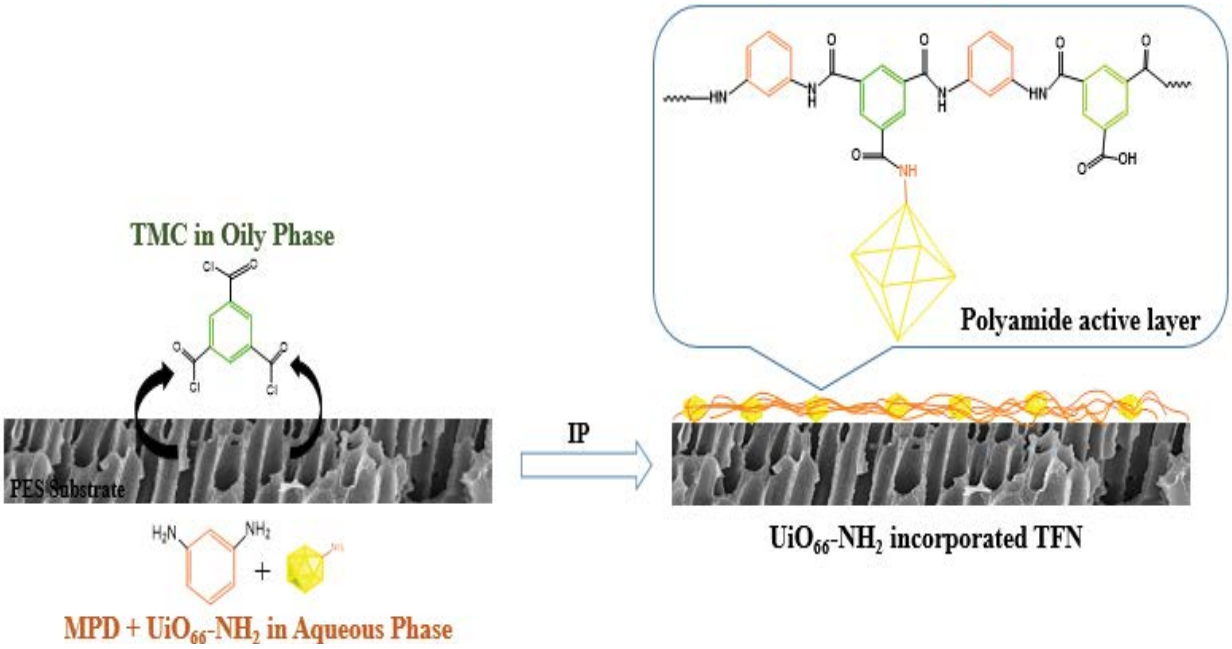

Fig. 1. Schematic representation of the synthetic route utilized for the fabrication of $UiO_{66}^{NH_2}$-modified TFN membranes via the IP process.

of lab-synthesized $UiO_{66}^{NH_2}$, scanning electron microscopy (SEM, Tescan, VEGA) was used. X-ray diffraction (XRD) measurements were also applied for the determination of the structure of the prepared nanofiller.

2.8. Membranes characterization

The surface composition of the PES substrate, control TFC and TFN membranes was studied by using attenuated total reflectance-Fourier transform infrared (ATR-FTIR) spectroscopy (Bruker, Equinox 15 55). The surface wetting properties of the lab-fabricated PES substrate and all the fabricated membranes (TFC and $UiO_{66}^{NH_2}$ modified TFN-FO membranes) were determined by contact angle goniometry (Dataphysics, OCA 15 plus) in triplicate. The surface roughness of the prepared membranes was measured by using atomic force microscopy (AFM; ENTEGRA AFMNT-MDT) by scanning an effective area of 5 μm × 5 μm. Morphological characteristics of the membranes were qualitatively assessed by SEM analysis (SEM, Tescan, VEGA).

3. Results and discussion

3.1. Characterization of $UiO_{66}^{NH_2}$ nanoparticle

ATR-FTIR measurements were carried out to identify the functional groups on the $UiO_{66}^{NH_2}$ nanoparticle. According to Fig. 2a, the characteristic absorption band at 3,344 cm^{-1} corresponds to the stretching mode of $–NH_2$ groups, and the vibration peaks present at 1,260 and 1,440 cm^{-1} are originated from C–N bonds. The peaks at 1,400; 1,510; 1,580; and 1,660 cm^{-1} can be assigned to the aromatic ligands. The asymmetric C–O vibration band at 1,574 cm^{-1} was

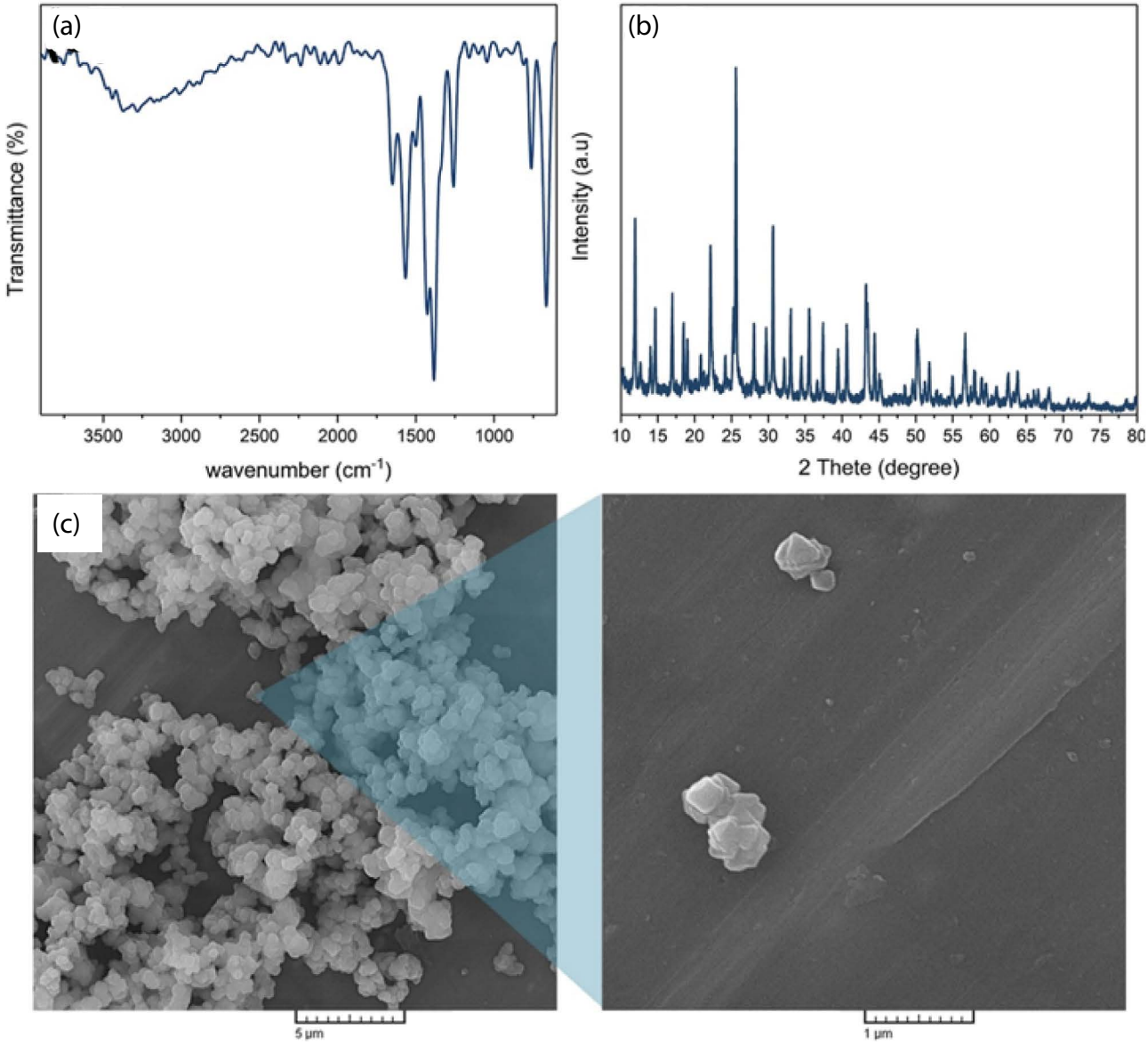

Fig. 2. (a) FTIR, (b) XRD, and (c) SEM characterization of $UiO_{66}^{NH_2}$.

detected in ATR-FTIR of $UiO_{66}^{NH_2}$, which indicates the presence of –COOH (NH_2–BDC ligand) in the obtained framework structure [30,31]. As can be seen in Fig. 2b, the crystalline structure of the as-fabricated $UiO_{66}^{NH_2}$ was evaluated by XRD experiments. The sharp peaks at 12° and 25° was observed in the XRD pattern, confirming that the as-synthesized nanoparticles were consistent with the simulated reference for $UiO_{66}^{NH_2}$ [24].

Fig. 1c presents the SEM morphology of the as-prepared nanoparticles, showing 3D structure of octahedrally cubic-like intergrown nanocrystals, similar to the previous work on $UiO_{66}^{NH_2}$ [32]. As shown in Fig. 1c, the nanoparticles average sizes of $UiO_{66}^{NH_2}$ were approximately 200 nm.

3.2. Characteristics of PES membrane sublayer

In the current study, the PA active layer of composite membranes has been fabricated on highly porous PES ultrafiltration substrates through the IP process. Since support layer features in terms of top, bottom, and cross-section morphologies, surface roughness and hydrophilicity affect the final morphology, and also FO performance of composite membranes, it is vital to specify these characteristics before the PA layer formation. Fig. 3 illustrates the cross-section, top, and bottom image of PES sublayer. As can be seen, the PES membrane has a finger-like cross-section morphology formed with a high degree of sub-micrometer pores. This cross-section morphology alleviate the structural parameter (S) for the membrane substrate [33,34]. The bottom SEM image presents a highly porous surface with large pores. A more porous bottom is estimated to improve the water and solute diffusion across the membrane. In addition, the top surface SEM image confirms the desirable features of the membrane-supporting layer for the fabrication of a highly efficient FO skin rejection layer via the IP process. The porosity of the membrane support layer has a substantial role in controlling the internal concentration polarization (ICP). Gravimetric experiments also confirm that the PES membrane sublayer possesses a high porosity of 73% ± 1.5%. The roughness and hydrophilicity of the membrane substrate were also analyzed by using AFM and water contact angle (WCA) tests, by which it was shown that the PES sublayer was relatively hydrophilic (75°) and smooth (R_a~12 nm).

3.3. Characterization of PA thin film

Membrane wettability behavior was investigated by using the static WCA as shown in Fig. 4b. Compared with pure TFC, the WCA of the $UiO_{66}^{NH_2}$ incorporated TFN-FO membranes was lower and presented a decreasing propensity as the $UiO_{66}^{NH_2}$ concentration increased in the PA rejection layer. As a result, by increasing the $UiO_{66}^{NH_2}$ concentration from 100 to 800 ppm in the MPD solution phase, the WCA decreased from 73.2° for TFN-U_{100} to 55.3° for TFN-U_{800}. The improved hydrophilicity of TFN-FO membranes might be related to the hydrophilic nature of the $UiO_{66}^{NH_2}$ nanofiller, which is placed at the top surface of the TFN membranes [20].

However, there was a little increase in WCA at $UiO_{66}^{NH_2}$ loading concentration more than 800 ppm. This might be due to aggregation of $UiO_{66}^{NH_2}$ nanoparticles (at high loading amounts of the nanofillers) during the IP process.

Fig. 5 shows the ATR-FTIR spectra of the modified TFN and the unmodified TFC composite membranes. The characteristic absorption peaks of the PES substrate can be easily found in all the membrane samples. As can be seen in Fig. 3, the spectra of the composite membranes present several new peaks corresponding to the PA thin film. The board peaks at 3,100–3,450 cm^{-1} are assigned to the –OH and –NH stretching bands. The peaks observed at 1,540 and 1,660 cm^{-1} are ascribed to the –NH and –CO stretching vibration of amide groups, respectively [35,36]. These observations confirm the successful formation of the PA thin film. The characteristic peaks of the $UiO_{66}^{NH_2}$ nanoparticles in TFN membranes are less obvious due to the overlap with the PA layer peaks.

However, confirmation on the incorporation of $UiO_{66}^{NH_2}$ within the PA thin film was concluded by EDS test as shown in Fig. 4a.

Figs. 6 and 7 display the top and cross-sectional SEM images of the TFC and TFN membranes. As observed in many previous studies, a ridge and valley structure was

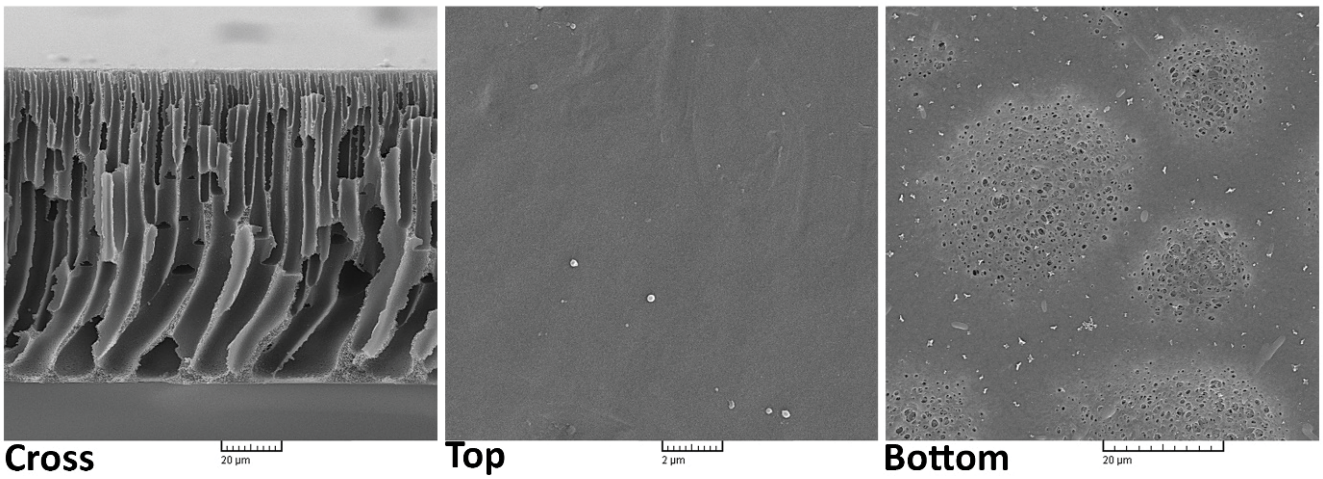

Fig. 3. Cross, top, and bottom SEM images of the PES membrane substrate.

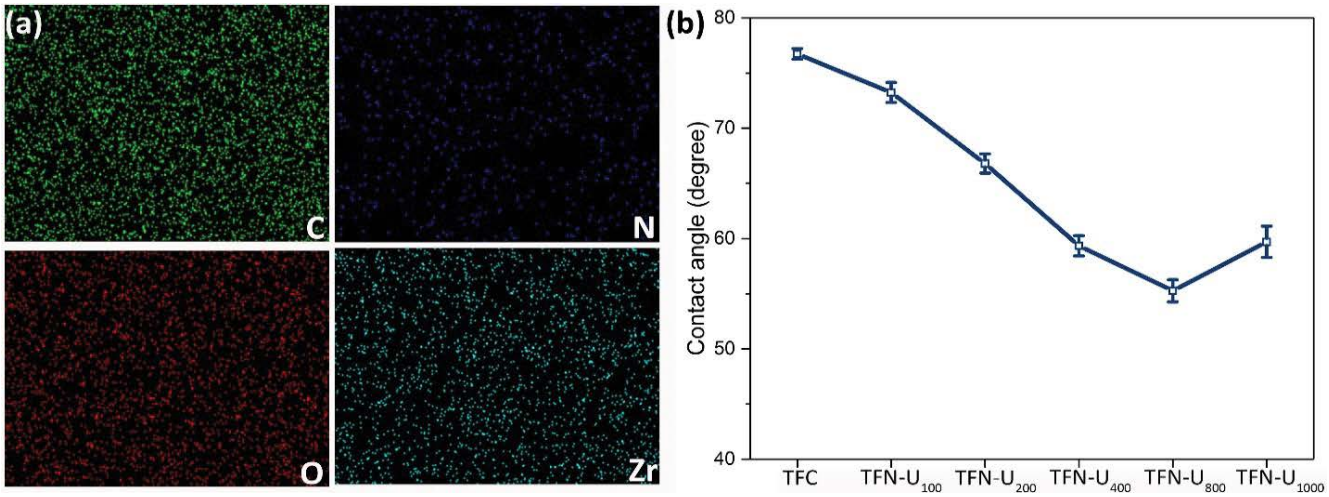

Fig. 4. (a) EDX analysis of TFN-U_{800} membrane and (b) WCA of different composite membranes.

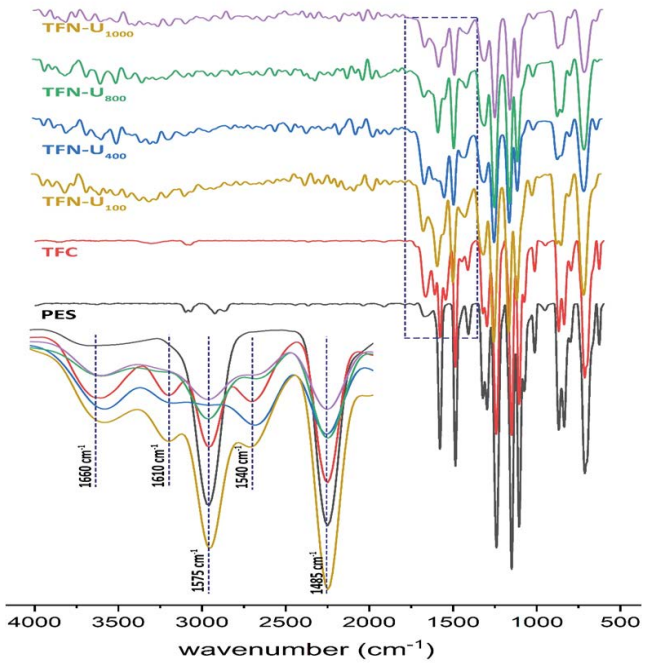

Fig. 5. FTIR spectra of different TFN membranes.

generated by the interfacial reaction of TMC and MPD monomers for all the PA thin films [37]. It can be seen that, the control TFC membrane presents a rough surface morphology. On the other hand, by introducing the $UiO_{66}^{NH_2}$ nanofiller into the PA thin film, a smoother surface morphology can be obtained. The thickness and roughness of the PA thin film also decrease with the increase in $UiO_{66}^{NH_2}$ loading in the MPD aqueous solution. This observation was similar to the previously reported works, in which it was found that hydrophilic additives in the PA layer could produce a thinner and smoother active layer [14–16].

These results suggest that the incorporation of $UiO_{66}^{NH_2}$ can affect the formation of the PA layer during the IP process. For the unmodified TFC membrane, MPD monomers can easily transfer from substrate pores to the reaction area with no limitation, leading to the formation of a thick and rough PA thin film. The $UiO_{66}^{NH_2}$ nanoparticles incorporated in TFN-FO membranes can retard the IP reaction due to the hydrogen bonding between the primary amine groups of $UiO_{66}^{NH_2}$ and the amine functional groups of MPD monomers [38,39]. Consequently, a thin and smooth thin film with a leaf-like morphology is obtained for the $UiO_{66}^{NH_2}$-modified PA thin film.

The AFM topographic images of the TFC and TFN-FO membranes, shown in Fig. 8, were used to further study the effect of the $UiO_{66}^{NH_2}$ nanofiller on the roughness of the PA thin film. Consistent with the SEM results, the surface roughness of the TFC membrane slightly changes after incorporating the $UiO_{66}^{NH_2}$ nanofiller within the PA thin film. As can be seen in 3D AFM images, the TFN-FO membranes presents low surface roughness compared to the control TFC membrane. The average surface roughness value (R_a) gradually decreases from 82 nm for the pristine TFC membrane to 66 nm for the TFN-U_{800} membrane. Based on the reported results in the previous similar study, incorporation of hydrophilic nanofillers into the active layer can reduce the surface roughness [40]. This can be related to the limitation of the migration of MPD monomers to the reaction side during the IP reaction.

3.4. FO performance of TFC and TFN membranes

The effect of $UiO_{66}^{NH_2}$ loading on the FO performance of TFN membranes, as depicted in Fig. 9, was investigated by using a draw solution of 1 M NaCl aqueous solution and a feed solution of DI water at 25°C. Increasing the loading of $UiO_{66}^{NH_2}$ within the PA active layer from 0 to 800 ppm led to a corresponding rise in water flux from 16.4 to 24.8 LMH, while the reverse salt flux was maintained low at about 2.8 gMH. The maintenance of reverse salt flux proposed that the rise of water flux was occurred due to the membrane defect caused from the incorporation of $UiO_{66}^{NH_2}$. This enhanced water flux could be attributed to the thin PA layer combined with high surface hydrophilicity of the TFN-U_{800} membrane. On the other hand, further

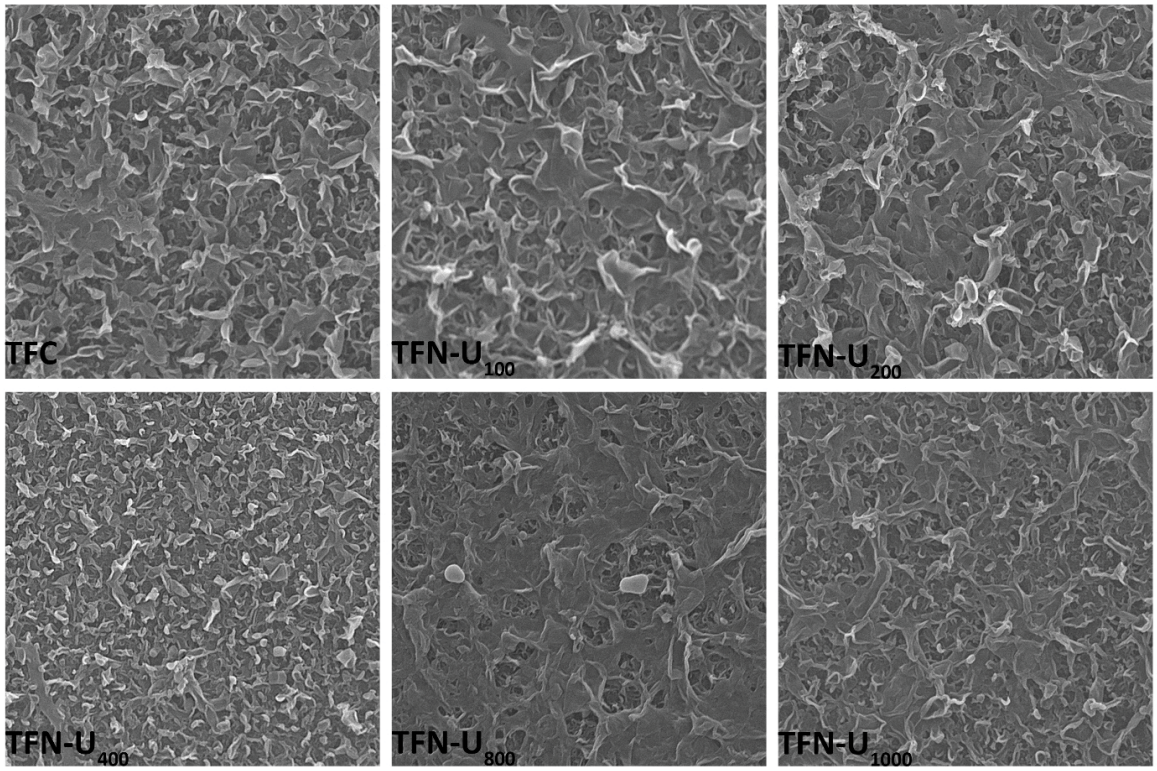

Fig. 6. Morphology of top surface of TFN membranes with different loading.

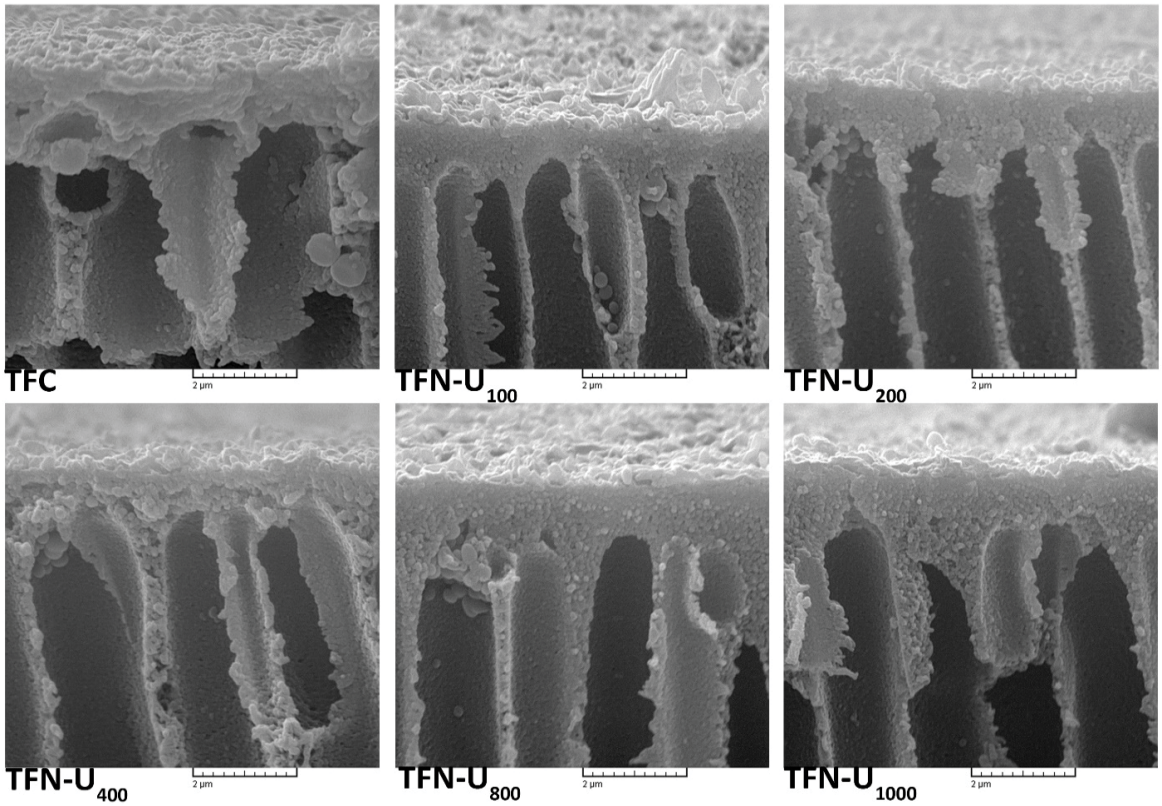

Fig. 7. Cross-section SEM images of PA layer of TFN membranes.

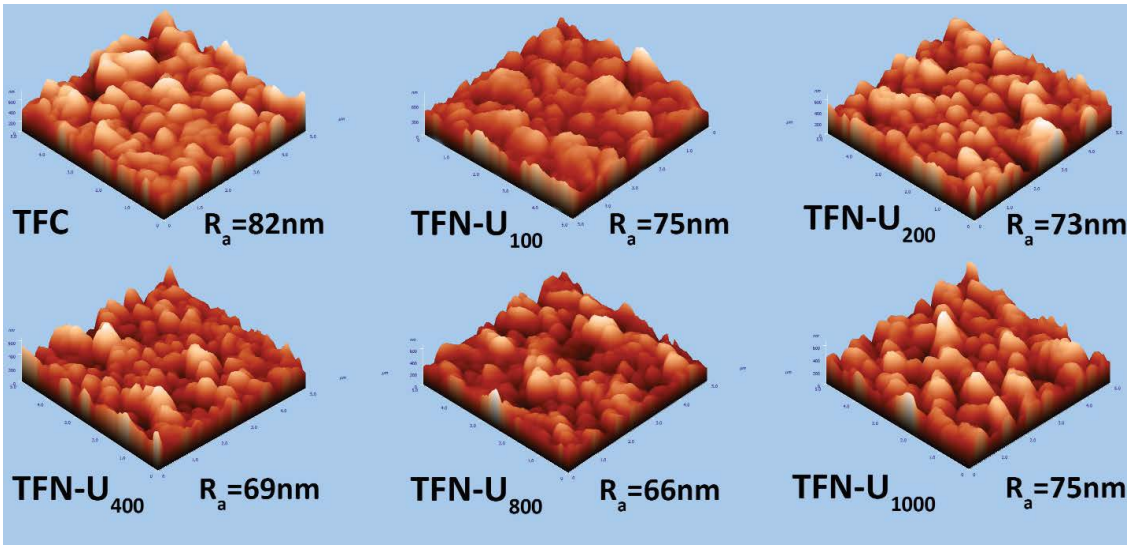

Fig. 8. 3D AFM images of TFN membranes with different concentration of $UiO_{66}^{NH_2}$.

raising the $UiO_{66}^{NH_2}$ loading to 1,000 ppm proved no longer effective, as the water flux dropped to 20.7 LMH, although the reverse salt flux remained low. This trend in water flux and reverse salt flux may have occurred because of three factors: (1) the decline of the membrane surface roughness declines water flux, (2) a decline of the thickness of the PA rejection layer also rises water flux, and (3) the rise of the membrane hydrophilicity usually rises the water flux [41,42]. Therefore, the combination of these property changes appeared to cause the net result of the water flux observed in Fig. 9a. The J_s/J_w ratio of the TFN membrane, an important selectivity parameter of a semipermeable FO membrane, is noticeably lower in comparison with the control TFC membrane, as shown in Fig. 9b. A lower J_s/J_w ratio is generally considered as a desirable condition for enhanced salt rejection, and a reduced amount of draw solute loss in the FO process. The experimental results reveal that the TFN-U800 membrane displays a maximum selectivity (J_s/J_w = 0.12 g/L). A further increase in $UiO_{66}^{NH_2}$ incorporation in the PA structure causes a significant reduction in selectivity for the TFN-U_{1000} membrane. This observable reduction in selectivity trends might be due to the unwanted defect created at the PA structure.

3.5. Evaluation of Cr(III) ion rejection

According to the separation performance data, the TFN-U_{800} membrane exhibits much better water flux and stable reverse solute flux, suggesting that the TFN-U_{800} membrane is the best choice to treat Cr^{3+} metal ions in FO experiment. Fig. 10 shows water flux and rejection efficiency of Cr^{3+} ions with different concentrations in FO configuration. For the Cr^{3+} concentration in the feed solution ranging from 500 to 2,000 ppm, the water flux decreased by 15%–35%. The lower water flux in higher concentrations of Cr^{3+} can be ascribed to the net driving force across the PA layer where the 2,000 ppm feed solution has a lower osmotic pressure difference in comparison to the 500 ppm one. In addition, the adsorption of Cr^{3+} to the MOF fillers leads to a decline in the size of water flow channel and consequently the water flux in the membrane. Different concentrations of Cr^{3+} in feed solutions have no effects on rejection of Cr^{3+} (Fig. 9). The rejection of Cr^{3+} remains as high as above 99.5% even in the high concentration of the feed solution (2,000 ppm). This superior rejection of the TFN-U_{800} membrane can be attributed to the presence of $UiO_{66}^{NH_2}$ in the active layer, which functions by two different mechanisms: (1) strong complexation between the primary amine groups of $UiO_{66}^{NH_2}$ and the Cr^{3+} ions and (2) providing an additional pathway for water molecules. Therefore, during the FO process, the porous and hydrophilic $UiO_{66}^{NH_2}$ nanofiller in the TFN-U_{800} membrane provides a selective transporting pathway for water molecules, and hence, accelerates the permeation of water molecules.

In addition, the presence of abundance amine groups in $UiO_{66}^{NH_2}$ structure can prevent the penetration of Cr^{3+} ions through the PA thin film by the strong complexation reaction.

4. Conclusion

In this work, the $UiO_{66}^{NH_2}$ nanofiller was synthesized and incorporated within the PA layer of the composite membrane by using the traditional interfacial polymerization of MPD/$UiO_{66}^{NH_2}$ and TMC monomers. The effect of embedment of $UiO_{66}^{NH_2}$ on the separation performance and physicochemical properties of the PA layer was completely investigated by using several instrument characterizations. This modification improved water flux of the TFN membranes, not only by raising the surface hydrophilicity but also through declining the thickness of the rejection layer. The effect of the $UiO_{66}^{NH_2}$ concentration on the performance of the TFN membranes in terms of water flux and reverse salt flux was examined, and the optimum FO performance (J_w = 24.8 LMH, J_s = 3.1 gMH) and the highest selectivity (J_s/J_w = 0.12 g/L) were observed for the membrane modified with 800 ppm $UiO_{66}^{NH_2}$. For that reason, the TFN-U_{800} membrane was used for treating the feed solution containing heavy metal Cr^{3+} ions in the FO operation. Furthermore,

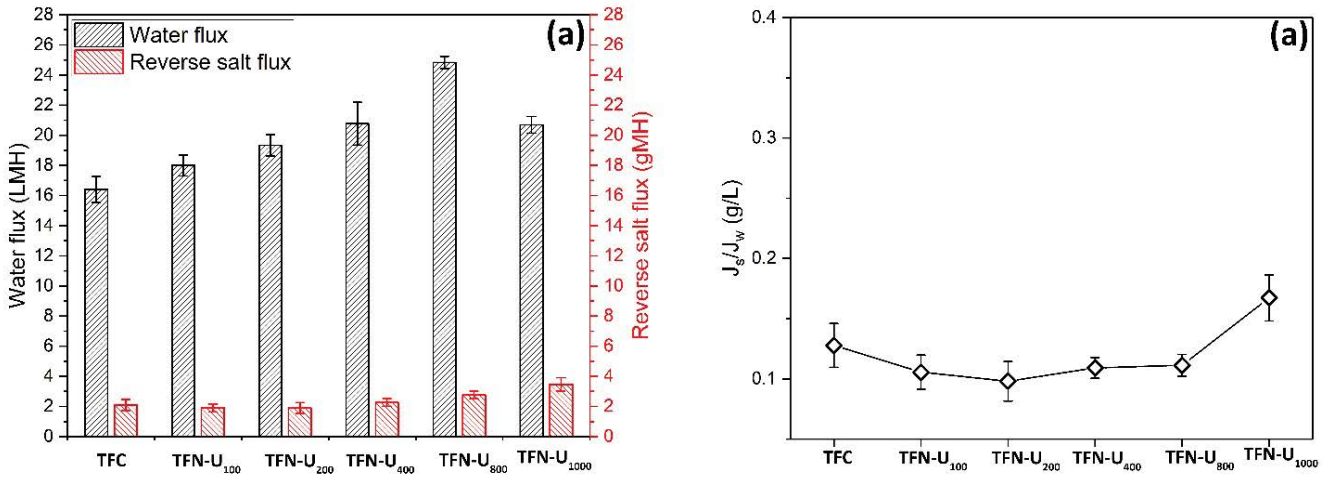

Fig. 9. FO performance of different TFN membranes: (a) water flux and reverse salt flux and (b) specific reverse salt flux.

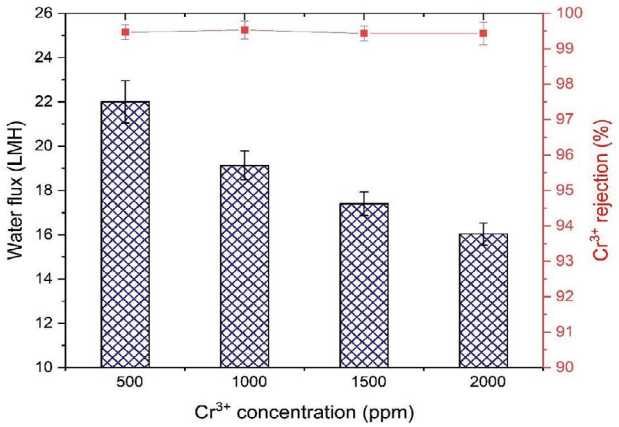

Fig. 10. Water and Cr^{3+} rejection in FO process.

the TFN-U_{800} membrane showed as high rejection propensity to Cr^{3+} ions (>97%) in the FO separation experiment. The $UiO_{66}^{NH_2}$ modified method in current research provided a promising strategy for preparing the effective PA active layers to develop the high-performance TFN-FO membranes in other heavy metals wastewater treatment.

Acknowledgments

The authors gratefully acknowledge the financial and instrumental supports received from the University of Tehran.

References

[1] H.F. Wen, C. Yang, D.G. Yu, X.Y. Li, D.F. Zhang, Electrospun zein nanoribbons for treatment of lead-contained wastewater, Chem. Eng. J., 290 (2016) 263–272.
[2] M.A. Alaei Shahmirzadi, S.S. Hosseini, J. Luo, I. Ortiz, Significance, evolution and recent advances in adsorption technology, materials and processes for desalination, water softening and salt removal, J. Environ. Manage., 215 (2018) 324–344.
[3] O. Ozay, S. Ekici, Y. Baran, N. Aktas, N. Sahiner, Removal of toxic metal ions with magnetic hydrogels, Water Res., 43 (2009) 4403–4411.
[4] J. Huang, M. Ye, Y. Qu, L. Chu, R. Chen, Q. He, D. Xu, Pb(II) removal from aqueous media by EDTA-modified mesoporous silica SBA-15, J. Colloid Interface Sci., 385 (2012) 137–146.
[5] Y. Qi, L. Zhu, X. Shen, A. Sotto, C. Gao, J. Shen, Polythyleneimine-modified original positive charged nanofiltration membrane: removal of heavy metal ions and dyes, Sep. Purif. Technol., 222 (2019) 117–124.
[6] Q. Chen, W. Xu, Q. Ge, Novel multicharge hydroacid complexes that effectively remove heavy metal ions from water in forward osmosis processes, Environ. Sci. Technol., 52 (2018) 4464–4471.
[7] X. Wei, X. Kong, S. Wang, H. Xiang, J. Wang, J. Chen, Removal of heavy metals from electroplating wastewater by thin-film composite nanofiltration hollow-fiber membranes, Ind. Eng. Chem. Res., 52 (2013) 17583–17590.
[8] F. Soyekwo, Q. Zhang, R. Gao, Y. Qu, C. Lin, X. Huang, A. Zhu, Q. Liu, Cellulose nanofiber intermediary to fabricate highly-permeable ultrathin nanofiltration membranes for fast water purification, J. Membr. Sci., 524 (2017) 174–185.
[9] A. Saeedi-Jurkuyeh, A.J. Jafari, R.R. Kalantary, A. Esrafili, A novel synthetic thin-film nanocomposite forward osmosis membrane modified by graphene oxide and polyethylene glycol for heavy metals removal from aqueous solutions, React. Funct. Polym., 146 (2020) 104397–104408.
[10] M. Qiu, C. He, Efficient removal of heavy metal ions by forward osmosis membrane with a polydopamine modified zeolitic imidazolate framework incorporated selective layer, J. Hazard. Mater., 367 (2019) 339–347.
[11] C. Liu, X. Lei, L. Wang, J. Jia, X. Liang, X. Zhao, H. Zhu, Investigation on the removal performances of heavy metal ions with the layer-by-layer assembled forward osmosis membranes, Chem. Eng. J., 327 (2017) 60–70.
[12] C.Y. Wu, H. Mouri, S.S. Chen, D.Z. Zhang, M. Koga, J. Kobayashi, Removal of trace-amount mercury from wastewater by forward osmosis, J. Water Process Eng., 14 (2016) 108–116.
[13] M. Rastgar, A. Shakeri, A. Karkooti, A. Asad, R. Razavi, M. Sadrzadeh, Removal of trace organic contaminants by melamine-tuned highly cross-linked polyamide TFC membranes, Chemosphere, 238 (2020) 124691–124701.
[14] A. Shakeri, H. Salehi, S.R. Razavi, S.M. Mirahmadi Babaheydari, Blue lemon@quaternary graphene oxide open frameworks: as a novel nanostructure for performance enhancement of thin film nanocomposite forward osmosis membrane, Chem. Eng. Res. Des., 148 (2019) 451–459.
[15] A. Shakeri, H. Salehi, F. Ghorbani, M. Amini, H. Naslhajian, Polyoxometalate based thin film nanocomposite forward osmosis membrane: superhydrophilic, anti-fouling, and high water permeable, J. Colloid Interface Sci., 536 (2019) 328–338.

[16] A. Shakeri, R. Razavi, H. Salehi, M. Fallahi, T. Eghbalazar, Thin film nanocomposite forward osmosis membrane embedded with amine-functionalized ordered mesoporous silica, Appl. Surf. Sci., 481 (2019) 811–818.
[17] X. Zhao, C. Liu, Efficient removal of heavy metal ions based on the optimized dissolution-diffusion-flow forward osmosis process, Chem. Eng. J., 334 (2018) 1128–1134.
[18] D. Ma, S.B. Peh, G. Han, S.B. Chen, Thin-film nanocomposite (TFN) membranes incorporated with super-hydrophilic metal-organic framework (MOF) UiO-66: toward enhancement of water flux and salt rejection, ACS Appl. Mater. Interfaces, 9 (2017) 7523–7534.
[19] Y. He, Y.P. Tang, D. Ma, T.S. Chung, UiO-66 incorporated thin-film nanocomposite membranes for efficient selenium and arsenic removal, J. Membr. Sci., 541 (2017) 262–270.
[20] F. Xiao, X. Hu, Y. Chen, Y. Zhang, Porous Zr-based metal-organic frameworks (Zr-MOFs)-incorporated thin-film nanocomposite membrane toward enhanced desalination performance, ACS Appl. Mater. Interfaces, 11 (2019) 47390–47403.
[21] L. Yang, Z. Wang, J. Zhang, Zeolite imidazolate framework hybrid nanofiltration (NF) membranes with enhanced permselectivity for dye removal, J. Membr. Sci., 532 (2017) 76–86.
[22] D. Ma, G. Han, S.B. Peh, S.B. Chen, Water-stable metal-organic framework UiO-66 for performance enhancement of forward osmosis membranes, Ind. Eng. Chem. Res., 56 (2017) 12773–12782.
[23] F. Xiao, B. Wang, X. Hu, S. Nair, Y. Chen, Thin film nanocomposite membrane containing zeolitic imidazolate framework-8 via interfacial polymerization for highly permeable nanofiltration, J. Taiwan Inst. Chem. Eng., 83 (2018) 159–167.
[24] X. Zhang, Y. Zhang, T. Wang, Z. Fan, G. Zhang, A thin film nanocomposite membrane with pre-immobilized UiO-66-NH_2 toward enhanced nanofiltration performance, RSC Adv., 9 (2019) 24802–24810.
[25] Y. Li, J. Liu, K. Zhang, L. Lei, Z. Lei, UiO-66-NH_2@PMAA: a hybrid polymer-MOFs architecture for pectinase immobilization, Ind. Eng. Chem. Res., 57 (2018) 559–567.
[26] H. Sun, B. Tang, P. Wu, Development of hybrid ultrafiltration membranes with improved water separation properties using modified superhydrophilic metal-organic framework nanoparticles, ACS Appl. Mater. Interfaces, 9 (2017) 21473–21484.
[27] A. Shakeri, H. Salehi, M. Rastgar, Chitosan-based thin active layer membrane for forward osmosis desalination, Carbohydr. Polym., 174 (2017) 658–668.
[28] T.M. Salehi, M. Peyravi, M. Jahanshahi, W.J. Lau, A.S. Rad, Impacts of zeolite nanoparticles on substrate properties of thin film nanocomposite membranes for engineered osmosis, J. Nanopart. Res., 20 (2018) 1–15, doi: 10.1007/s11051–018–4154–1.
[29] P. Zhao, B. Gao, Q. Yue, S. Liu, H.K. Shon, The performance of forward osmosis in treating high-salinity wastewater containing heavy metal Ni^{2+}, Chem. Eng. J., 288 (2016) 569–576.
[30] X.F. Zhang, Y. Feng, Z. Wang, M. Jia, J. Yao, Fabrication of cellulose nanofibrils/UiO-66-NH_2 composite membrane for CO_2/N_2 separation, J. Membr. Sci., 568 (2018) 10–16.
[31] X. Guo, D. Liu, T. Han, H. Huang, Q. Yang, Pyrolysis of heavy oil in the presence of supercritical water: the reaction kinetics in different phases, AICHE J., 61 (2015) 857–866.
[32] J. Pang, Z. Kang, R. Wang, B. Xu, X. Nie, L. Fan, F. Zhang, X. Du, S. Feng, D. Sun, Exploring the sandwich antibacterial membranes based on UiO-66/graphene oxide for forward osmosis performance, Carbon, 144 (2019) 321–332.
[33] N.N. Bui, J.T. Arena, J.R. McCutcheon, Proper accounting of mass transfer resistances in forward osmosis: improving the accuracy of model predictions of structural parameter, J. Membr. Sci., 492 (2015) 289–302.
[34] G. Han, T.S. Chung, M. Toriida, S. Tamai, Thin-film composite forward osmosis membranes with novel hydrophilic supports for desalination, J. Membr. Sci., 423–424 (2012) 543–555.
[35] M. Rastgar, A. Shakeri, H. Salehi, Study of polyamide thin film characteristics impact on permeability/selectivity performance and fouling behavior of forward osmosis membrane, Environ. Sci. Pollut. Res., 26 (2019) 1181–1191.
[36] H. Salehi, A. Shakeri, M. Rastgar, Carboxylic polyethersulfone: a novel pH-responsive modifier in support layer of forward osmosis membrane, J. Membr. Sci., 548 (2018) 641–653.
[37] S. Abdikheibari, W. Lei, L.F. Dumée, N. Milne, K. Baskaran, Thin film nanocomposite nanofiltration membranes from amine functionalized-boron nitride/polypiperazine amide with enhanced flux and fouling resistance, J. Mater. Chem. A, 6 (2018) 12066–12081.
[38] H. Sun, P. Wu, Tuning the functional groups of carbon quantum dots in thin film nanocomposite membranes for nanofiltration, J. Membr. Sci., 564 (2018) 394–403.
[39] H. Zarrabi, M.E. Yekavalangi, V. Vatanpour, A. Shockravi, M. Safarpour, Improvement in desalination performance of thin film nanocomposite nanofiltration membrane using amine-functionalized multiwalled carbon nanotube, Desalination, 394 (2016) 83–90.
[40] S.H. Kim, S.Y. Kwak, B.H. Sohn, T.H. Park, Design of TiO_2 nanoparticle self-assembled aromatic polyamide thin-film-composite (TFC) membrane as an approach to solve biofouling problem, J. Membr. Sci., 211 (2003) 157–165.
[41] W. Zhao, H. Liu, Y. Liu, M. Jian, L. Gao, H. Wang, X. Zhang, Thin-film nanocomposite forward-osmosis membranes on hydrophilic microfiltration support with an intermediate layer of graphene oxide and multiwall carbon nanotube, ACS Appl. Mater. Interfaces, 10 (2018) 34464–34474.
[42] J. Zhu, L. Qin, A. Uliana, J. Hou, J. Wang, Y. Zhang, X. Li, S. Yuan, J. Li, M. Tian, J. Lin, B. Van der Bruggen, Elevated performance of thin film nanocomposite membranes enabled by modified hydrophilic MOFs for nanofiltration, ACS Appl. Mater. Interfaces, 9 (2017) 1975–1986.